Journal of Structural Geology 30 (2008) 761–766

Contents lists available at ScienceDirect

Journal of Structural Geology

journal homepage: www.elsevier.com/locate/jsg

Normal fault inversion by orthogonal compression: Sandbox experiments with weak faults

F.O. Marques [a,*], C.R. Nogueira [b]

[a] Universidade de Lisboa, Faculdade de Ciencias, Departamento de Geologia and CGUL-IDL, Lisboa, Portugal
[b] Universidade de Lisboa, Faculdade de Ciencias, Departamento de Geologia, Lisboa, Portugal

ARTICLE INFO

Article history:
Received 4 October 2007
Received in revised form 9 February 2008
Accepted 24 February 2008
Available online 4 March 2008

Keywords:
Sedimentary basin
Graben
Normal fault inversion
Weak fault
Orthogonal compression
Sandbox experiments

ABSTRACT

Linear frictional failure criteria predict that normal faults form dipping around 60°, and reverse faults around 30°, depending on dry rock properties. Therefore, it is unlikely that normal faults be reactivated as reverse faults, unless the stress conditions are favourable, or the intrinsic properties of the intact rock or of the precursor fault (PF) are modified. In the present study, we focused on friction (strength) of the PF. We used sandbox experiments with an initially embedded weak PF dipping 60° or 70°, filled with a thin film of silicone putty that lubricated the (weak) fault, to investigate inversion of high angle PF by orthogonal compression. The results show that: (1) the PF can be inverted if it is weak during compression, even if the angle of dip is as great as 70°; (2) after inversion initiation, the reverse movement on the PF can last for as much as 30% model shortening, leading to great amounts of reverse displacement along the PF before the formation of a thrust ahead; (3) in models with more than one PF, the weakness of the reactivated fault closer to piston was not enough to prevent reactivation of the PF further ahead, after an amount of shortening that depended on distance between PFs.

The viscous material used to weaken the fault is scalable to salt in nature. However, the great decrease in friction due to lubrication with a viscous material can simulate many other weakening mechanisms observed in nature.

1. Introduction

The inversion of grabens has received great attention in the past two to three decades, because (1) of the important economic role played by inverted structures in petroleum generation and trapping; (2) most deformation in the brittle upper crust is accommodated by the reactivation of existing faults rather than by the creation of new faults; and (3) of the mechanical problem raised by inversion of high angle precursor faults (PF). Sibson (1985) showed that in nature, for typical rock friction coefficients, it is unlikely that high angle normal faults be reactivated as high angle reverse faults, unless the effective least principal stress is tensile and/or the friction coefficient is abnormally low. Brun and Nalpas (1996) showed experimentally that normal fault inversion occurs only when the angle of inversion is less than 45°. Despite these results, many authors have tried to simulate normal fault inversion by orthogonal compression using sandbox experiments. However, they have been, with no exception, unsuccessful. Even Sassi et al. (1993) and Panien et al. (2005), who made the normal faults weaker prior to shortening, did not succeed in producing significant reverse movement (if any) in the PFs. Therefore, we start by analyzing why.

The most intuitive way to do this is by using the Mohr diagram (Fig. 1). Dry quartz sand has negligible cohesion (e.g. Hubbert, 1951; Schellart, 2000), hence the fracture line for intact sand goes through the origin of the coordinate system. Despite the many determinations of the angle of internal friction (ϕ) of sand, we use a very commonly used $\phi = 35°$ (e.g. Hubbert, 1951). With such a construction, it is clear that normal faults cannot be reactivated by orthogonal compression when pure dry quartz sand is used. Increase of σ_1 during compression at constant σ_3 (dashed half circles in Fig. 1) makes the Mohr circle touch the fracture line for intact sand much before the point corresponding to the precursor normal fault does. Then a great deal of the Mohr circle will be inside the instability field (stresses greater than needed to form a fault). Therefore, less differential stress is required to form a new, low angle reverse fault (thrust), than to reactivate the PF. Even if one argues that a PF is weaker than intact sand because of dilation, the difference is not that significant (e.g. Sassi et al., 1993). The angle ϕ for the PF would be only slightly less than 35°, and hence much less work would be necessary to create a new thrust. Therefore, to invert precursor normal faults in a sandbox (or in nature), changes must

* Corresponding author. Tel.: +351 217500000; fax: +351 217500064.
E-mail address: fomarques@fc.ul.pt (F.O. Marques).

0191-8141/$ – see front matter © 2008 Elsevier Ltd. All rights reserved.
doi:10.1016/j.jsg.2008.02.015

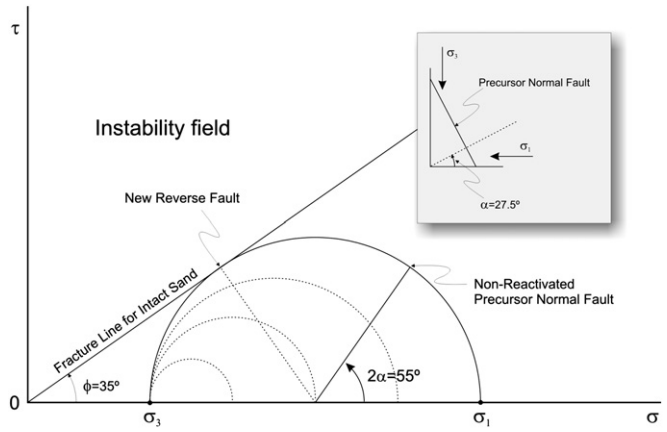

Fig. 1. Mohr diagram for sand. Increase of σ_1 during compression at constant σ_3 (dashed half circles) makes the Mohr circle touch the fracture line for intact sand much before the point corresponding to the precursor normal fault. Therefore, a low angle reverse fault forms instead of reactivation of the precursor high angle fault.

occur in σ_3 and/or in the intrinsic properties of the fault as indicated by Sibson (1985).

Possible solutions are the use of fluid overpressure and/or weak faults, as a first approximation, to significantly change the intrinsic properties of pure dry quartz sand or of PFs. The effects of overpressure have been studied with sandbox experiments by, e.g., Cobbold and Castro (1999) and Mourgues and Cobbold (2003). In the present study, we investigate the effects of fault weakening on the inversion of high angle PFs by orthogonal compression, by lubricating the fault surface (much lower coefficient of friction). In order to weaken the fault, we insert a thin layer of silicone putty on the fault, which substantially decreases the friction on the fault surface and can simulate widespread weakening mechanisms and be compared directly with salt injection in natural faults. It is not the aim of the present study to discuss weakening mechanisms; we just take as premise that they exist and can be simulated with a weak analogue material.

We used sandbox modelling to investigate the: (1) effects of fault weakening on inversion of high angle PFs during shortening; (2) amount of dip slip displacement during inversion; and (3) inversion in a model with more than one PF. We did not carry out a first phase of extension of the model to make the normal faults (similar to Sassi et al., 1993); for practical and strategic reasons, we used models with initially embedded weak faults whose angle of dip is typical for normal faults that form in nature and in sandbox experiments, which is between 50° and 70°.

2. Experimental method

2.1. Scaling

We chose a length ratio (model over nature) $l_r = l_m/l_n = 5.0 \times 10^{-6}$, so that a brittle crust 10 km thick scales down to a model layer ca. 50 mm thickness. Our models were 400 mm long, 100 mm wide and 50 mm deep (Fig. 2), thus representing 80 km × 20 km × 10 km in nature. We chose a strain rate ratio $(v_m/l_m)/(v_n/l_n) \approx 10^9$, so that a prototype velocity (v) of about 0.44 cm yr^{-1} (ca. 1.4×10^{-8} m s^{-1}) scales down to ca. 7.0×10^{-5} m s^{-1} in the models.

For the convenience of PDMS as geological model material, in particular as analogue of rock salt, we rely on the detailed analyses of Weijermars (1986) and Weijermars et al. (1993).

2.2. Model materials

To model the brittle upper crust, we used a Coulomb material, natural quartz sand from Fontainebleau, with grain size of ca. 300 μm, density of ca. 1.3×10^3 kg m^{-3}, very low cohesion and an angle of internal friction between 30° and 40°, as in brittle rock (e.g. Hubbert, 1951). For better definition of faults, Galland et al. (2006) and Coelho et al. (2006) used silica powder. For the present experiments, normal sand seemed appropriate. However, ongoing work on fault reactivation by our group will use silica powder. For the viscous filling of the PF (in some experiments also at the base of the sand pack), we used polydimethylsiloxane (PDMS – Dow Corning SGM36), which, at room temperature, has a density of ca. 0.965×10^3 kg m^{-3}, is Newtonian (at the applied strain rate) and has a viscosity of about 5×10^4 Pa s.

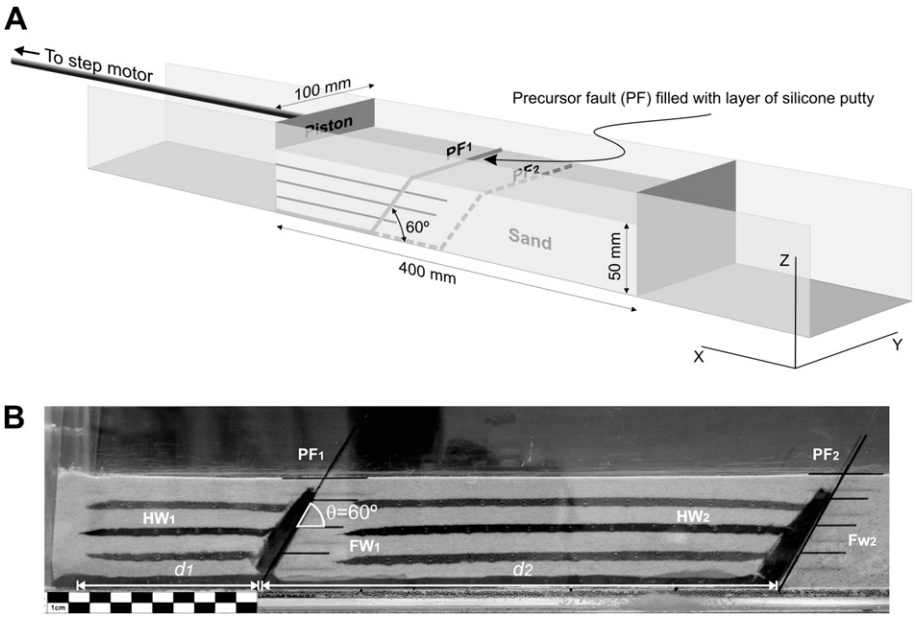

Fig. 2. (A) Sketch of geometry and layer distribution in the experimental models. (B) Side view of initial stage. PF_1 and PF_2 are precursor faults closest to and furthest from piston. HW_1 and HW_2 are hanging walls to PF_1 and PF_2, respectively.

2.3. Apparatus, boundary conditions and model construction

The experiments were performed in a Perspex rectangular box, in which three vertical walls were fixed and one was mobile (Fig. 2). This acted as a piston and was pushed by a computer controlled stepping motor at a steady velocity of about 7.0×10^{-5} m s^{-1}, so shortening the model. The models without basal PDMS comprised a sand pack of 50 mm thickness on average with an initial flat top surface (no intentional initial perturbations). The models with basal PDMS comprised a sand pack of 50 mm thickness with a 5 mm layer of PDMS at the base, between the piston and the PF (Fig. 2). Thin coloured sand layers with acrylic micro beads were added as markers to trace fault movement and displacement paths during fault inversion. PFs with embedded PDMS were introduced in the model before compression; they dipped $\theta \approx 60^\circ$ or 70° towards piston with strike orthogonal to piston movement. We did not simulate sedimentation and/or erosion processes during the runs. This is a subject for further investigation. The model was in dry frictional contact with the walls, or in viscous frictional contact with the basal plate in models with basal PDMS layer. The fault also worked as viscous frictional.

Four main model configurations were designed (Table 1, Figs. 6 and 7), with PFs dipping $\theta \approx 60^\circ$: (1) one weak fault (in one experiment we tested $\theta \approx 70^\circ$); (2) two parallel weak faults; (3) partial basal viscous layer together with one weak fault; and (4) partial basal viscous layer together with two weak faults. The influence of distance between faults and piston (d) was also tested. The distance between the piston and the nearest PF is designated as d_1 and the distance between the two parallel PFs is d_2.

3. Experimental results

Faults and displacements were monitored using digital time-lapse imaging through the transparent sidewalls. Displacement vector maps were constructed as in Marques and Cobbold (2002), at 3% model shortening intervals, using markers and time-lapse imaging.

3.1. Model 1 – one weak fault, $\theta \approx 60$ or 70°, no basal viscous layer

These experiments were designed to test the influence of PF distance from piston on fault reactivation and hanging wall block behaviour. Three different types of experiments were run with the PF embedded in the model at distances $d_1 \approx 100$, 150 or 175 mm. One type of experiment was run with $\theta \approx 70^\circ$ and PF placed at $d_1 \approx 100$ mm to test inversion of a very high angle weak fault.

Shortening in the very early stages (<2% shortening) was accommodated by sand thickening, which propagated forward from the piston. If there was diffuse reverse faulting along d_1, it was not perceptible. Inversion of the PF took place in all models before 5% shortening, although weakly for $d_1 \approx 175$ mm. PF inversion initiated earlier (ca. 2.2% model shortening) in experiments with $d_1 \approx 100$ mm, including with PF dipping $\theta \approx 70^\circ$ (Fig. 3B). Inversion initiation was well marked by the development of a fault scarp at the surface tip of the PF. Further inversion could be evaluated by displacement of markers. Brittle failure of the hanging wall block took place in experiments with $d_1 \approx 100$ mm and $\theta \approx 60^\circ$ or 70°, but only after 5% model shortening; i.e. inversion preceded thrusting in the hanging wall. In both experiments, a backthrust formed rooting at the bottom tip of the PF (Fig. 3A and B). For $d_1 \approx 175$ mm and similar amount of shortening (2.2%), a thrust formed dipping 35° towards the piston; while for $d_1 \approx 100$ mm it initiated when the PF was also inverted, for $d_1 \approx 175$ mm thrust formation preceded inversion of the PF.

Model shortening was mostly accommodated by displacement along the PF, by flattening of sand in the hanging wall and by thrusts (fore or back). Hanging wall thickening and absence of erosion increased the taper angle to unrealistic values. Nevertheless, inversion was long living, without any visible signs of footwall deformation (thickening and/or brittle failure).

3.2. Model 1a – one weak fault, $\theta \approx 60^\circ$, viscous layer at the base of hanging wall block

This model was designed to investigate the influence of a basal viscous layer on fault inversion. PDMS worked as a lubricant, thus facilitating slip of sand over basal Perspex. Model 1 comprised two types of experiments: $d_1 \approx 100$ or 150 mm.

Table 1
Model configuration

Model	Configuration	Parameters	Objectives	Results
1	One weak PF and basal dry friction	$\theta \approx 60^\circ$ or 70°, $d_1 \approx 100$, 150 or 175 mm	Reactivation of one weak PF over dry frictional basal detachment	Figs. 3 and 6
1a	One weak PF and viscous layer at base of hanging wall block	$\theta \approx 60^\circ$, $d_1 \approx 100$ or 150 mm	Reactivation of one weak PF over viscous low frictional basal detachment	Figs. 5b and 7
2	Two weak PFs and basal dry friction	$\theta \approx 60^\circ$, $d_1 \leq 150$ mm $d_2 \approx 200$ or 250 mm	Reactivation of two parallel weak PFs separated by different d_2, over dry frictional basal detachment	Fig. 4
2a	Two weak PFs and viscous layer at base of hanging wall blocks	$\theta \approx 60^\circ$, $d_1 \leq 150$ mm $d_2 \approx 200$ or 250 mm	Reactivation of two parallel weak PFs separated by different d_2, over viscous low frictional basal detachment	Fig. 5

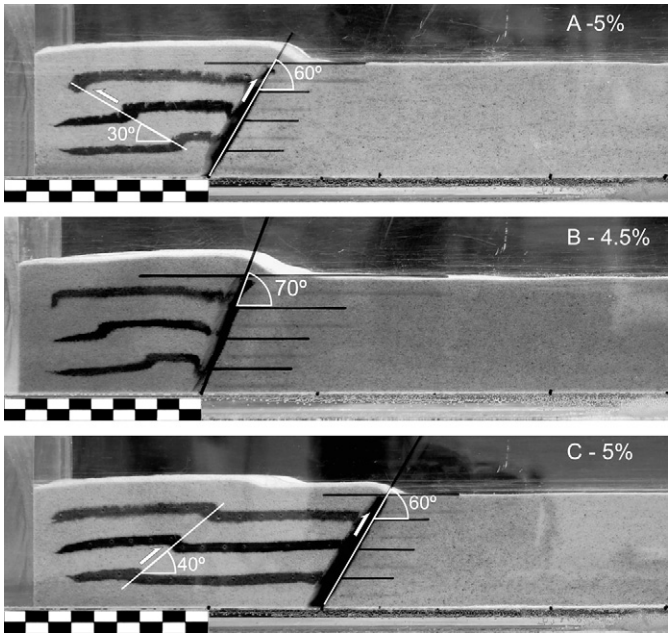

Fig. 3. Sidewall views of Model 1, where piston moved from left to right. (A) $\theta \approx 60^\circ$ and $d_1 \approx 100$ mm. (B) $\theta \approx 70^\circ$ and $d_1 \approx 100$ mm. (C) $\theta \approx 60^\circ$ and $d_1 \approx 150$ mm. PDMS thickness is greatly exaggerated due to drag and spreading on Perspex wall.

In Model 1a, PF inversion took off slightly earlier than in Model 1, so that at identical model shortening the marker layers and fault scarp showed greater vertical displacement. At 5% model shortening, no backthrust was observed. Instead, a blind short-living forethrust formed for $d_1 \approx 100$ mm. Regarding $d_1 \approx 150$ mm, a forethrust formed simultaneously with PF inversion and kept active for a longer period, until 20% model shortening. PF inversion proceeded with faster growth when compared to Model 1, which can be evaluated by the amount of fault displacement for identical model shortening. Inversion was long living without any perceptible signs of footwall deformation till ca. 17% model shortening. At this stage, a short-living thrust formed rooting at the upper half of the PF, emerging underneath the overdeveloped scarp fault for $d_1 \approx 150$ mm. Despite this small thrust, inversion of the PF was active well after 17% model shortening.

3.3. Model 2 – two weak faults, $\theta \approx 60^\circ$, no basal viscous layer

These experiments were designed to test if model shortening (read inversion) could propagate forwards to more than one weak fault. PF_1 and PF_2 designate the PFs closest to and furthest from piston, respectively. HW_1 and HW_2 designate hanging walls of PF_1 and PF_2, respectively. Two types of experiments were used to analyse the effects of d_2 on inversion of PF_2: $d_2 \approx 200$ mm or 250 mm.

The initial shortening stages of both experiments were similar to Model 1 with $d_1 \leq 150$ mm, because the used d_1 was similar. PF_1 was active and HW_1 was thickening on both experiments until c.a. 20% of model shortening. Reactivation of PF_2 took off at ca. 22% model shortening. From this stage onwards, inversion of PF_1 was blocked and HW_1 worked as a rigid piston. Inversion of PF_2 proceeded without brittle failure (visible) of HW_2 for $d_2 \approx 200$ mm until 30% of model shortening was reached, when a backthrust developed in HW_2, rooting at the bottom tip of PF_2 and reaching the surface in front of PF_1 fault scarp (Fig. 4B). For $d_2 \approx 250$ mm, a short-living thrust formed in HW_2 at ca. 25% model shortening (a bit earlier than for $d_2 \approx 200$ mm), rooting at the base of the model and followed by the development of a backthrust that rooted at the bottom tip of PF_2.

3.4. Model 2a – two weak faults, $\theta \approx 60^\circ$, viscous layer at the base of hanging wall blocks

This model comprised two types of experiments, $d_2 \approx 200$ or 250 mm, with other conditions as in Model 2.

The initial shortening stages were very similar to Model 1a, because d_1 was similar. PF_1 was active until c.a. 20% model shortening. After this stage, inversion of PF_1 and deformation within HW_1 were blocked and HW_1 behaved as a rigid piston. Reactivation of PF_2 took off earlier than in Model 2, showing evident inversion with greater scarp development at 20% model shortening (Fig. 5C).

When compared to Model 2 experiments, where d_2 of both faults were similar, inversion of both PFs took place for lower values of shortening, without visible signs of footwall deformation. Also, no perceptible reverse faulting occurred in HW_2 during the entire shortening. PF inversion proceeded with faster growth when compared to Model 2 experiments.

3.5. Displacement maps

We present displacement maps for two typical experiments and for different amounts of model shortening, in order to show strain under different conditions and at different deformation stages without recourse to a great amount of pictures.

At 3% model shortening, displacement vectors show that: (1) the *X* component gradually vanishes away from the piston, with a clear step at the thrust fault; (2) the *Z* component increases from the bottom to the top, and gradually vanishes away from the piston; (3) PF inversion was very small for this shortening value; (4) the thrust, at this stage, dipped 35°; (5) no deformation of the PF footwall was observed, therefore, all model shortening was concentrated in the PF hanging wall, which means that effective shortening (calculated over d_1 and not over whole model length, which we call model shortening) was around 11%.

After 6% model shortening, displacement vectors show some significant differences from the previous stage: (1) in the thrust hanging wall, vectors rotated toward horizontal (thus higher angle to the thrust); in the footwall, the *Z* component decreased at the base close to the thrust, where there is almost a pure *X* component, and increased significantly and gradually towards the top and the PF, becoming approximately parallel to the weak fault; (2) at this stage, PF and thrust movements were similar, and shortening was being accommodated in great part by displacement along faults; (3) after less than 5% shortening, the thrust had steepened by 10°; (5) still no deformation of the PF footwall was observed.

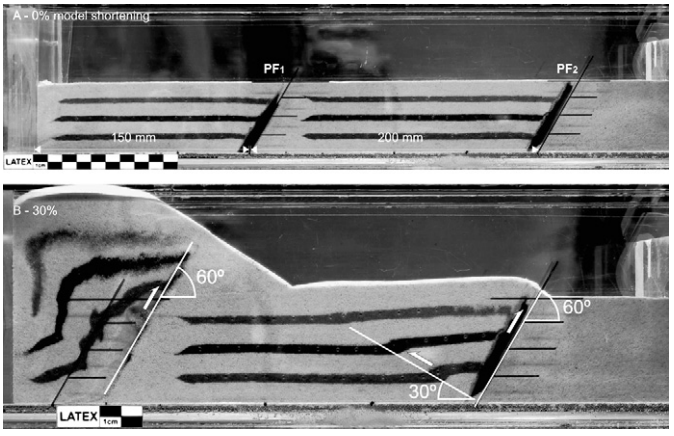

Fig. 4. Sidewall views of Model 2, where piston moved from left to right. (A) initial stage with $\theta \approx 60^\circ$, $d_1 \approx 150$ mm and $d_2 \approx 200$ mm. (B) deformation at 30% model shortening.

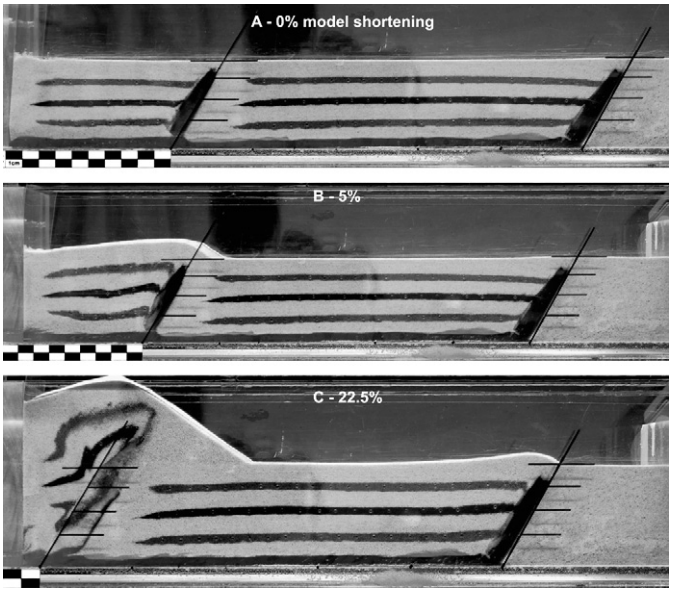

Fig. 5. Sidewall views of Model 2a, where piston moved from left to right. (A) initial stage with $\theta \approx 60^\circ$, $d_1 \approx 100$ mm and $d_2 \approx 250$ mm. (B) deformation at 5% model shortening. C – Deformation at 22.5% model shortening.

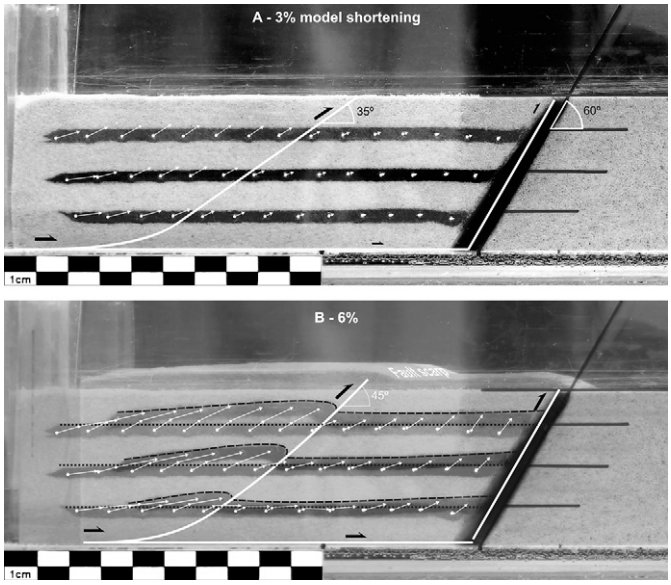

Fig. 6. Displacement maps for Model 1 constructed from markers and time-lapse imaging. Dotted and dashed lines in B highlight marker layers before and after deformation, respectively. Note the very small PF inversion at 3% model shortening; most shortening is hence accommodated by sand thickening and displacement along the thrust. At 6% model shortening, displacement along PF was similar to displacement along the thrust, which had already steepened by 10°.

At 3% model shortening, displacement vectors show that: (1) the *X* component gradually vanishes away from the piston, with a small step at the thrust fault; (2) the *Z* component increases from the bottom to the top, and gradually vanishes away from the piston till midway in the thrust footwall, where the *Z* component appreciably increases towards the PF; (3) PF inversion was significant for this shortening value; (4) shortening was accommodated by sand thickening and displacement along both thrust and PF; (5) at this stage, the thrust dipped 35°; (5) no deformation of the PF footwall was observed.

The map integrating displacements between 3 and 15% model shortening shows that: (1) displacement in the thrust hanging wall was approximately rectilinear, with trajectories dipping around 24° in average, thus oblique to the thrust; (2) displacement at the base of the thrust footwall was mostly horizontal (pure translation); (3) displacement in the footwall immediately below the thrust was oblique and low dipping; (4) displacement closer to the PF gradually rotated and became parallel to the weak fault; (5) the thrust steepened by 25° in this interval; (6) still no deformation of the PF footwall could be observed.

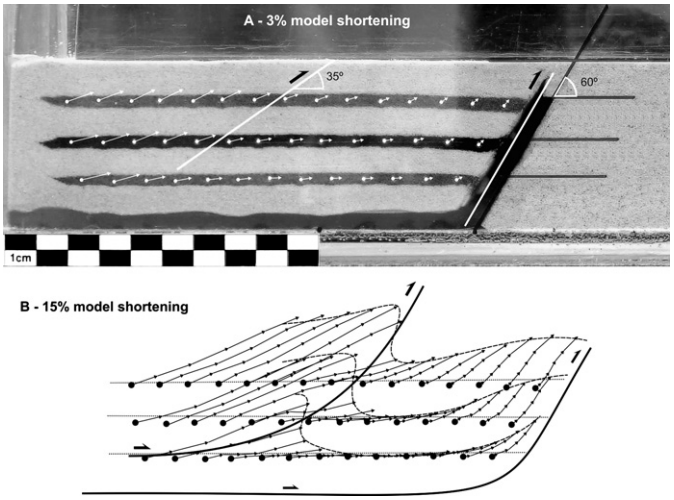

Fig. 7. Displacement maps for Model 1a constructed from markers and time-lapse imaging. Dotted and dashed lines in B represent marker layers before and after deformation, respectively. Note significant PF inversion at 3% model shortening; most shortening is hence accommodated by displacement along thrust and PF. At 15% model shortening, the thrust had already steepened by 25°.

4. Discussion

Formation of a thrust in the PF footwall occurred only after ca. 20% model shortening for $d_1 \approx 100$ mm and after ca. 30% for $d_1 \geq 150$ mm. This means that the inverted weak PF could take up a great deal of shortening and be active for great amounts of model shortening. Therefore, effective shortening (PF hanging wall shortening) is much greater than model shortening. Erosion of the hanging wall topography could have prolonged the activity in the inverted PF because the taper angle would be decreased by erosion (Storti and McClay, 1995; Corrado et al., 1998; Koyi et al., 2000; Marques and Cobbold, 2002, 2006).

Thrust faults in the experiments formed at low angles but gradually rotated towards steep dips with increased shortening of the hanging wall block. Some became inactive at relatively low amounts of shortening (see also Mulugeta and Koyi, 1992; Koyi, 1995). Flattening of sand in the hanging wall block (uniform strain with vertical extension and horizontal contraction) seems to be mostly responsible for the observed thrust rotation. A complementary explanation can be sand compaction (e.g. Koyi et al., 2003). However, as noted by Weijermars et al. (1993), volume change in sand inside fault blocks is negligibly small (<2.5%).

The thickness of the PDMS layer in the fault is irrelevant because the velocity was very low and constant. Thickness of the viscous layer cannot change its viscosity, but a very thick viscous layer would shorten horizontally and extrude at the surface before actual fault reactivation with up throw of hanging wall block, and a very thin viscous layer would make the fault much stronger, which is the opposite of our premise. Sand grains would be strongly agglutinated by the highly viscous PDMS and cohesion would hence increase drastically. In terms of rigorous scaling, the used PDMS thickness is obviously exaggerated. In order to keep scaling, the fault would be strong instead of weak. Therefore, we had to compromise between scaling and weak fault, by using a viscous layer as thin as possible. All that was needed was that sand grains on one side of the PDMS did not contact with the ones on the other side so as to avoid (greater) dry friction. The PDMS layer at the base of the model was used to decrease friction, as it happens in nature with salt and/or (fluid) over pressured rocks. As shown by the experimental results, this had some effects on PF inversion: (1) transmit the piston movement further into the model by decreasing basal resistance, thus inverting the PF at smaller model shortening values; (2) lift the hanging wall block up because of PDMS thickening; (3) migrate into the PF thus contributing to the inversion of the weak fault.

Analysis of the displacement maps shows that: (1) non-parallelism between vectors and faults indicate that both horizontal translation and sand flattening (*X* contraction and *Z* expansion) took place in the deforming sand block. In Model 1, the considerable change in vector orientation toward lower dips was the result of PF inversion, which at 6% model shortening was as much active as the thrust. This accommodated a great deal of model shortening, thus slowing down both thrust movement and sand flattening in the thrust hanging wall block. Because of increased displacement along the PF, horizontal translation was increased away from the PF, helped by décollement at the basal contact of sand with Perspex. (2) Sand flattening is also attested by the observed thrust rotation. (3) Vectors at the base indicate PDMS thickening when they

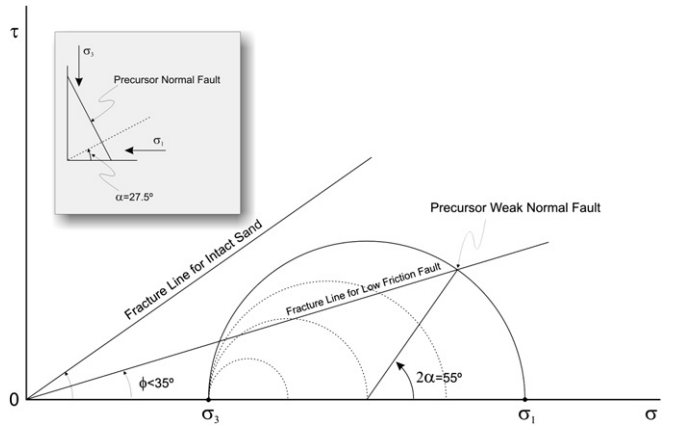

Fig. 8. Mohr diagram for the present experiments. Increase of σ_1 during compression with constant σ_3 (dashed half circles) made the Mohr circle touch the point for the PF on the Mohr circle before the Mohr circle reached the fracture line for intact sand. Therefore, inversion of the precursor high angle fault took less work than to form a low angle reverse fault.

incorporate a positive *Z* component, which is the case of the region between the piston and the footwall right below the thrust. The pure horizontal translation observed in between the faults means that there was no PDMS thickening in this region; therefore, PDMS was simple sheared and injected into the PF. This may have been helped by increased loading due to thickening of the hanging wall block. Comparison between displacement maps for Models 1 and 1a shows that basal viscous friction enhanced activity of PF and significantly changed the displacement pattern when compared to dry friction.

The present experiments show that the PDMS layer in the fault greatly decreased friction, so that it took less work to invert the PF than to create new thrusts in the footwall. On the Mohr diagram (Fig. 8), this means that the slope of the PF's fracture line was greatly decreased, such that the PF point on the Mohr circle was reached by the growing Mohr circle before the Mohr circle reached the fracture line for intact sand.

5. Conclusions

The present experiments show that orthogonal inversion is possible if the PF is significantly weak, so that the work needed to invert the PF is less than that needed to create a new thrust. In the Mohr diagram, the point on the circle corresponding to the PF must touch the PF fracture line before the Mohr circle reaches the fracture line for intact sand.

The present experimental results show that: (1) the PF can be inverted if it is weak during compression, even if the angle of dip is as great as 70°; (2) after inversion initiation, the reverse movement on the PF can last for a great amount of model shortening, leading to great amounts of dip slip displacement; (3) in models with more than one PF, the weakness of the reactivated PF closer to piston is not enough to prevent reactivation of the PF further ahead, after an amount of shortening that depends on distance between PFs; (4) friction was much lower in models with a basal viscous detachment, which promoted propagation of compressive stress further into the model, so producing reactivation earlier than in models with dry basal detachment (higher friction).

Acknowledgments

This is a contribution to research project TEAMINT (POCTI/CTE/48137/2002) funded by FCT. The experiments were carried out in the Experimental Tectonics Lab of LATTEX/IDL, University of Lisbon. Constructive reviews by O. Galland and H. Koyi, and editorial work by C. Passchier are gratefully acknowledged. CRN thanks FCT and Fundação Calouste Gulbenkian for fellowships.

References

Brun, J.P., Nalpas, T., 1996. Graben inversion in nature and experiments. Tectonics 15, 677–687.
Cobbold, P.R., Castro, L., 1999. Fluid pressure and effective stress in sandbox models. Tectonophysics 301, 1–19.
Coelho, S., Passchier, C., Marques, F.O., 2006. Riedel-shear control on the development of pennant veins: field example and analogue modeling. Journal Structural Geology 28, 1658–1669.
Corrado, S., Di-Bucci, D., Naso, G., Faccenna, C., 1998. Influence of paleogeography on thrust system geometries: an analogue modelling approach for the Abruzzi-Molise (Italy) case history. Tectonophysics 296, 437–453.
Galland, O., Cobbold, P.R., Hallot, E., de Bremond d'Ars, J., Delavaud, G., 2006. Use of vegetable oil and silica powder for scale modelling of magmatic intrusion in a deforming brittle crust. Earth Planetary Science Letters 243, 786–804.
Hubbert, M.K., 1951. Mechanical basis for certain familiar geologic structures. Geological Society of America Bulletin 62, 355–372.
Koyi, H., 1995. Mode of internal deformation in sand wedges. Journal of Structural Geology 17, 293–300.
Koyi, H.A., Hessami, K., Teixell, A., 2000. Epicenter distribution and magnitude of earthquakes in fold-thrust belts: insights from sandbox models. Geophysical Research Letters 27, 273–276.
Koyi, H.A., Sans, M., Teixell, A., Cotton, J., Zeyen, H., 2003. The significance of penetrative strain in the restoration of shortened layers: insights from sand models and the Spanish Pyrenees. In: McClay, K.R. (Ed.), Thrust Tectonics and Hydrocarbon Systems. AAPG Memoir, 82, pp. 1–16.
Marques, F.O., Cobbold, P.R., 2002. Topography as a major factor in the development of arcuate thrust belts: insights from sandbox experiments. Tectonophysics 348, 247–268.
Marques, F.O., Cobbold, P.R., 2006. Effects of topography on the curvature of fold-and-thrust belts during shortening of a 2-layer model of continental lithosphere. Tectonophysics 415, 65–80.
Mourgues, R., Cobbold, P.R., 2003. Some tectonic consequences of fluid overpressures and seepage forces as demonstrated by sandbox modelling. Tectonophysics 376, 75–97.
Mulugeta, G., Koyi, H., 1992. Episodic accretion and strain partitioning in a model sand wedge. Tectonophysics 202, 319–333.
Panien, M., Schreurs, G., Pfiffner, A.O., 2005. Sandbox experiments on basin inversion: testing the influence of basin orientation and basin fill. Journal of Structural Geology 27, 433–445.
Sassi, W., Colletta, B., Balé, P., Paquereau, T., 1993. Modelling of structural complexity in sedimentary basins: the role of pre-existing faults in thrust tectonics. Tectonophysics 226, 97–112.
Schellart, W.P., 2000. Shear test results for cohesion and friction coefficients for different granular materials: scaling implications for their usage in analogue modelling. Tectonophysics 324, 1–16.
Sibson, R.H., 1985. A note on fault reactivation. Journal of Structural Geology 7, 751–754.
Storti, F., McClay, K., 1995. Influence of syntectonic sedimentation on thrust wedges in analogue models. Geology 23, 999–1002.
Weijermars, R., 1986. Flow behaviour and physical chemistry of bouncing putties and related polymers in view of tectonic laboratory applications. Tectonophysics 124, 325–358.
Weijermars, R., Jackson, M.P.A., Vendeville, B., 1993. Rheological and tectonic modelling of salt provinces. Tectonophysics 217, 143–174.